Rula G. Abdallat[1,2]
Aziela S. Ahmad Tajuddin[1]
David H. Gould[1]
Michael P. Hughes[1]
Henry O. Fatoyinbo[1]
Fatima H. Labeed[1]*

[1]Faculty of Engineering and Physical Sciences, Centre for Biomedical Engineering, University of Surrey, Guildford, Surrey, United Kingdom
[2]The Hashemite University, Zarqa, Jordan

Received August 19, 2012
Revised December 27, 2012
Accepted January 2, 2013

Research Article

Process development for cell aggregate arrays encapsulated in a synthetic hydrogel using negative dielectrophoresis

Spatial patterning of cells is of great importance in tissue engineering and biotechnology, enabling, for example the creation of bottom-up histoarchitectures of heterogeneous cells, or cell aggregates for in vitro high-throughput toxicological and therapeutic studies within 3D microenvironments. In this paper, a single-step process for creating peelable and resilient hydrogels, encapsulating arrays of biological cell aggregates formed by negative DEP has been devised. The dielectrophoretic trapping within low-energy regions of the DEP-dot array reduces cell exposure to high field stresses while creating distinguishable, evenly spaced arrays of aggregates. In addition to using an optimal combination of PEG diacrylate pre-polymer solution concentration and a novel UV exposure mechanism, total processing time was reduced. With a continuous phase medium of PEG diacrylate at 15% v/v concentration, effective dielectrophoretic cell patterned arrays and photo-polymerisation of the mixture was achieved within a 4 min period. This unique single-step process was achieved using a 30 s UV exposure time frame within a dedicated, wide exposure area DEP light box system. To demonstrate the developed process, aggregates of yeast, human leukemic (K562) and HeLa cells were immobilised in an array format within the hydrogel. Relative cell viability for both cells within the hydrogels, after maintaining them in appropriate iso-osmotic media, over a week period was greater than 90%.

Keywords:
Cell encapsulation / Cell patterning / Dielectrophoresis / Hydrogels / Tissue engineering
DOI 10.1002/elps.201200459

1 Introduction

Current cell-based in vitro studies for drug efficacy are unreliable and non-predictive in a clinical setting, mainly due to the monolayer models (2D) employed [1]. Various techniques have been investigated to generate complex 3D cell–cell and cell–extracellular matrices (ECMs) capable of interactions, as would be seen in vivo [2, 3]. The field of tissue engineering allows for the fabrication of functionally complex and biomechanically stable tissue microstructures, with living cells being the building block. These ex vivo microstructures, maintained with appropriate scaffolding material, are of tremendous benefit in a variety of bioprocesses, such as localised culturing and high-throughput drug screening where assays such as drug binding, apoptosis, proliferation and cytotoxicity can be monitored in real time.

Since the development of soft contact lenses from poly(2-hydroxyethyl methacrylate) by Wichterle and Lim in the 1960s [4], a range of different hydrogels have been applied for biological applications including space-filling agents [5], drug delivery systems [6], biosensing systems [7] and cellular scaffolds that provide high water content when swollen, thus mimicking the 3D microenvironment of the ECM [8, 9]. The choice between a natural (e.g. collagen, fibrin) and a synthetic (e.g. PEG, polyacrylic acid) hydrogel is function and property specific, though biocompatibility issues such as immunogenic responses to animal-derived hydrogels, tend to favour the use of synthetic hydrogels in biological applications. Advantages of synthetic over natural hydrogels include photo-polymerisation, adjustable chemical composition influencing the mechanical properties (e.g. brittleness, scaffold arrangement) and mass transfer properties (e.g. diffusion of nutrient and metabolic waste) [2, 7, 9, 10]. PEG diacrylate (PEG-DA) is a commonly adopted synthetic hydrogel, formed when the functional hydroxyl end groups of the PEG macromer are converted to the functional group acrylate. This macromolecular precursor is photo-polymerised using UV

Correspondence: Dr. Henry O. Fatoyinbo, Faculty of Engineering and Physical Sciences, Centre for Biomedical Engineering, University of Surrey, Guildford, Surrey GU2 7XH, UK
E-mail: h.fatoyinbo@surrey.ac.uk
Fax: +44-1483-686736

Abbreviations: **CPM**, continuous phase mixture; **DMPA**, 2,2-dimethoxy-2-phenylacetophenone; **ECM**, cell–extracellular matrice; **nDEP**, negative DEP; **pDEP**, positive DEP; **PEG-DA**, PEG diacrylate; **UV**, ultraviolet

*Additional corresponding author: Dr. Fatima H. Labeed, E-mail: f.labeed@surrey.ac.uk

Colour Online: See the article online to view Fig. 1 in colour.

irradiation, at physiological temperature and pH, to form hydrogel scaffolds in situ whereby 3D constructs contain the dispersed immobilised bio-agent (e.g. cells). Factors such as photo-initiator concentration and structure, period of UV exposure and the macromolecule chain length and composition influence the hydrogel formation process [2, 11]. PEG-DA microspheres have been investigated for cell transplantation (i.e. islet of Langerhans), and found that immunoisolation of the encapsulated cells provided good diffusion properties for waste and nutrients for prolonged periods based on the thin-layered hydrogels formed [12, 13]. A technology that shows great potential in generating discrete, homogenous and heterogeneous, cell aggregates in a 3D microenvironment is DEP [14].

DEP occurs when an inhomogeneous electric field is applied to a solution in which polarisable particles are forced to move [15]. It is an attractive and inexpensive way of selectively manipulating heterogeneous populations of cells in microsystems, without deleterious effects to the cell [16]. The interaction between cell and the field non-uniformity generates an imbalance of bound charges at the cell-medium interface resulting in a net force on the cell [17]. Microelectrode geometries fabricated by photolithography generate large electric field gradients, from low amplitude voltages (<20 V), required to manipulate cells [18, 19]. Along with the field non-uniformity, the complex dielectric properties of both cell and surrounding medium affect the strength and direction of the DEP force [6, 18, 19]. Equation (1) shows the governing equation for the time-averaged DEP force ($\langle F_{\mathrm{DEP}} \rangle$) a spherical particle is subjected to, where ∇ is the gradient operator Del of the root mean square of the electric field (E_{RMS}), $\mathrm{Re}[K(\omega)]$ is the real part of the Clausius–Mossotti factor, $\varepsilon_{\mathrm{m}} = \varepsilon_0 \varepsilon_{\mathrm{r}}$ is the absolute permittivity of suspending medium, $\omega = 2\pi f$ is the angular frequency and r is the particle radius:

$$\langle F_{\mathrm{DEP}} \rangle = 2\pi r^3 \varepsilon_{\mathrm{m}} \mathrm{Re}[K(\omega)] \nabla |E_{\mathrm{RMS}}|^2 \quad (1)$$

The Clausius–Mossotti factor is a frequency-dependent complex quantity described by the complex permittivities ($\varepsilon_{\mathrm{i}}^* = \varepsilon_{\mathrm{i}} - j\frac{\sigma_{\mathrm{i}}}{\omega}$) of the medium (i = m) and particle (i = p), with the material's conductivity (σ_{i}) contributing to the frequency response. The Clausius–Mossotti factor is given by Eq. (2); where negative DEP (nDEP) is in the range $-0.5 < \mathrm{Re}[K(\omega)] < 0$ and directed towards low intensity fields while positive DEP (pDEP) is in the range $0 < \mathrm{Re}[K(\omega)] < 1$.

$$K(\omega) = \frac{\varepsilon_{\mathrm{p}}^* - \varepsilon_{\mathrm{m}}^*}{\varepsilon_{\mathrm{p}}^* + 2\varepsilon_{\mathrm{m}}^*} \quad (2)$$

DEP is extremely versatile and has been investigated for processes such as electrophysiology of biological particles [20–22], microfluidic operations including separation of heterogeneous populations of cells [23] and pre-concentration of biological material from environmental material [24]. Trapping cells in patterned arrays using DEP can be achieved with appropriate microelectrode designs. However, since the DEP force is temporary, upon field removal cells can re-disperse within the continuous phase. Immobilisation of cells after patterning can be achieved by cross-linking agents [25], biolithography [26] or trapping cells in constructs made from biomaterials (e.g. PEG wells) [27].

In this paper, a process route for hydrogel encapsulation of DEP patterned cell aggregates at low-energy field traps in our DEP-dot microsystem is presented. Through minimising cytotoxic conditions (physical, chemical and electrical) [28], optimal conditions for combining DEP patterning efficiencies and continuous phase viscosity were elucidated. Aggregate array formation was achieved through an energised microsystem situated in a compact, purpose-built portable UV light box for DEP experimentation, with viability studies carried out after hydrogel polymerisation on test biological cells.

2 Materials and methods

2.1 Design of near-UV irradiating DEP light box

Previous studies using DEP prior to hydrogel formation via photo-polymerisation reactions have used single point focussed UV beams to polymerise small regions or sequential regions at a time [10, 29]. This process raises issues of non-uniform cross-linkage in the hydrogel scaffold and timing issues. To reduce the process time, we designed and built in-house a portable UV irradiating enclosure (Fig. 1A) specifically designed to accommodate DEP experiments and to produce a single wide-area exposure of the pre-polymer suspension within the DEP-dot microsystem (Section 2.2) for uniform cross-linkage of the hydrogel. The DEP light box, measuring 150 mm (L) × 115 mm (H) × 220 mm (W), was made from aluminium, with two 4 W UV fluorescent tubes (F4T5BL350, BLT Direct) placed within the inside top of the box, 25 mm above the stage where DEP-dot microsystem resides, indicated by 1 within Fig. 1A. The UV tubes were wired to electronic starters (2) and mounted on to a holder (3) attached to a rail system, which allowed the tubes to be manually moved forward into position, directly above the DEP-dot microelectrode system, when turned on and backwards when turned off to allow image capture from a mounted camera. A side enclosure situated on the right-hand side was isolated from the UV-irradiated enclosure by a fitted panel, as shown in Fig. 1B. This housed the electric circuits of the UV light and fail-safe mechanism for the light box, automatically switching off the UV light if the door is opened. In addition, wires for dielectrophoretic experiments were threaded through the front panel of the side enclosure, along the bottom of the side enclosure and out through a 5 mm diameter rubber covered opening as indicated by the asterisk in Fig. 1B.

2.2 Fabrication of DEP microelectrode system

The microelectrode arrangement, as shown in Fig. 1C, is based on the 'DEP-dot' system design where the electric field morphology within a single dot has been evaluated [30]. The

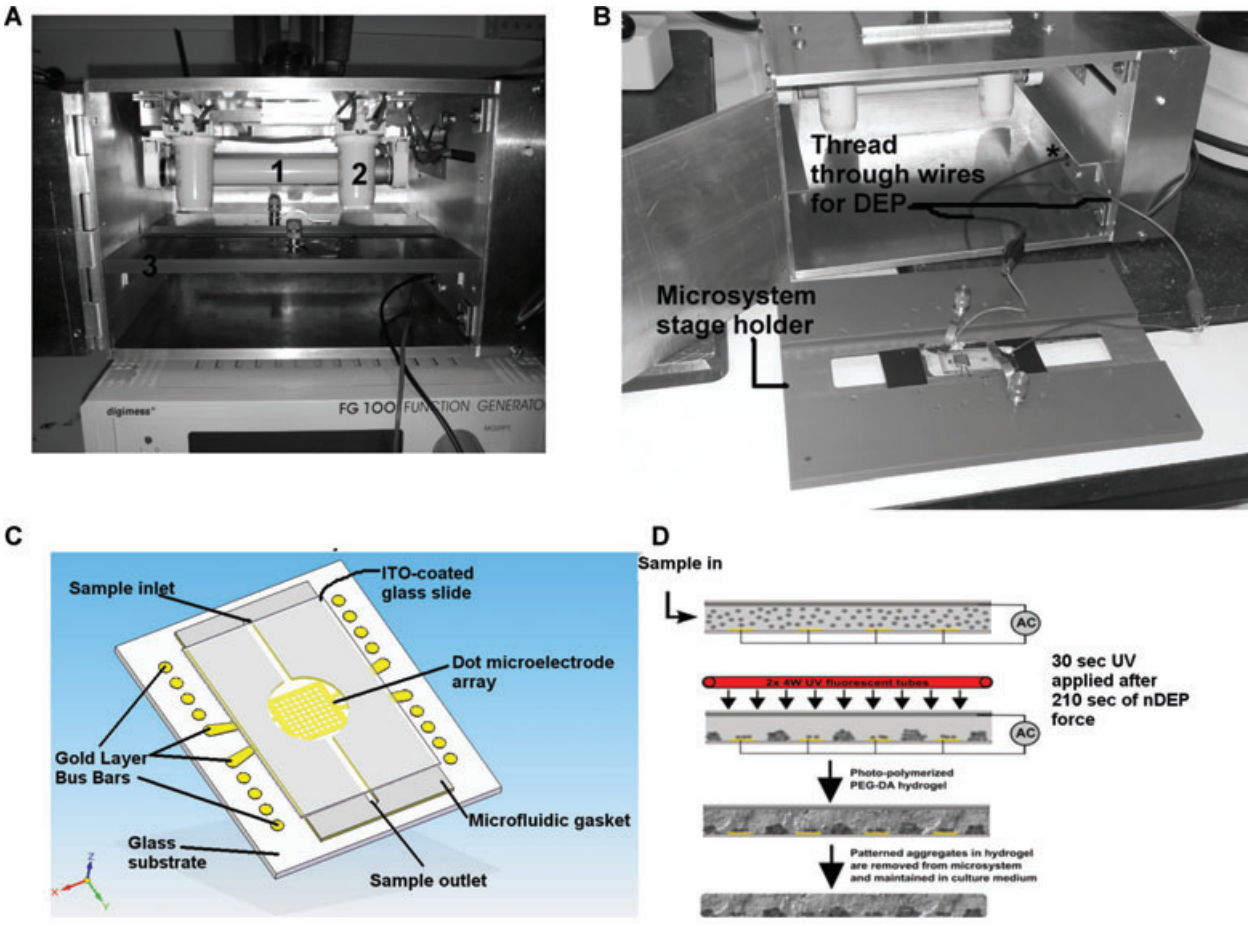

Figure 1. Photographs of the designed and manufactured portable, wide-area, light box for DEP experiments; (A) the light box on top of a digimess signal generator with the door open shows the position of the 4 W UV tubes (1) the electronic starter (2) and the position of the DEP stage holder (3) for positioning of the DEP-dot microsystem. (B) The microsystem stage holder removed from the large enclosure with a DEP-dot system residing on the stage. Threaded wires connected to a signal generator emerge from (*) and connect to the microsystem for DEP experiments; (C) CAD design of the microelectrode array used in experiments and the shape of the microfluidic gasket, separating the indium tin oxide counter-electrode from the dot microelectrode array by 300 μm; (D) schematic of the process for creating cell aggregates using nDEP within a DEP-dot microsystem and sequential encapsulation in PEG-DA via UV irradiation within the DEP light box.

system consists of two parallel facing planar electrodes on glass substrates, in which the top electrode is a transparent indium tin oxide layer (Delta Technologies, USA) and the bottom electrode is a gold layer comprising of discrete circular apertures, arranged in an array format. The thin film gold-coated (200 nm) microscope slides with titanium seed layer (20 nm) were obtained from the University of Sheffield (EPSRC Centre for III-V Technologies). Masks for the circular aperture (150–500 μm dia.) arrays were designed on commercially available CAD software (CorelDraw) and produced on high-resolution emulsion film (JD Photo-Tools, UK). Gold slides were cut to size (36 × 26 mm) of the mask designs and cleaned with 70% ethanol and DI water (Purite Select Analysis 40, Jencons). The dried slides were then spun coated with positive photoresist (Microposit S1813, Rohm and Haas) at 4000 rpm for 50 s. The photoresist covered slides were then soft-baked on a hot plate for 1 min at 100°C, and stored in a dark place for subsequent use within 24 h. Positive photolithographic processing was used to generate the circular apertures on the gold-coated slides. Using a commercially available PCB light box, pattern transfer unto the gold slide was accomplished. All surfaces (i.e. light box, masks and photoresist coated slides) were cleaned using an air duster to remove particulates before the photoresist coated surface and the mask surfaces were aligned in the light box. An opaque substrate was placed on top of the aligned structure to inhibit UV irradiation from above. UV irradiation, from the bottom fluorescent tubes, through the translucent regions of the masks lasted 40 s; the irradiated slides were then developed in 1:3 diluted photoresist developer (Microposit 351, Rohm and Haas) until the patterned geometries became visible and inspected under a light microscope. The slides were then hard-baked for 45 min in a Memmert oven at 90°C. The hard-baked slides were submerged in gold etchant (10% potassium iodide, 2.5% iodine, 18% hydrochloric acid) until the exposed gold regions were removed and then neutralised

with sodium thiosulphate and DI water. The titanium seed layer was removed in heated dilute hydrochloric acid and the remaining regions of photoresist were removed using photoresist stripper.

A mask for the gasket separating both top and bottom electrode and providing microfluidic channels towards and away from the microelectrode array, was designed in CAD and printed out on transparency slides on an office laser jet printer. An electrically insulating photo-polymer resin (Poly-Diam, UK) was UV cured producing a gasket thickness of 300 μm, which was sandwiched between top and bottom electrodes. Bus bar connections were made through silver epoxy (RS, UK) and electrical wires connected to a Digimess FG100 function generator (RS, UK). Figure 1D shows a side view schematic of the dot microsystem at successive stages of the process from cell aggregation through nDEP at the dot centres, irradiation of the microsystem within the DEP light box to form encapsulated cell aggregate arrays and removal of the photo-polymerised hydrogel from within the microsystem.

2.3 Continuous phase mixture (CPM)

All materials were purchased from Sigma Aldrich, UK unless stated otherwise. Pre-polymer PEG-DA(M_w = 575) was mixed with 280 mM D-mannitol solution at 10 different ratios, with PEG-DA concentrations varying by 5% between 5 and 50%. The photo-initiator 2,2-dimethoxy-2-phenylacetophenone (DMPA) was dissolved in 1-vinyl-2-pyrrolidone at 100 mg/mL, then mixed (Rotamixer, Hook & Tucker) with the pre-polymer/D-mannitol solution at a final volumetric concentration of 0.01% v/v. In instances where DEP experiments were performed, the solution was supplemented with potassium chloride (KCl) to obtain a continuous phase conductivity value of 7 mS/m as measured using a handheld conductivity meter (Jenway, UK).

2.4 Cell culturing

Yeast (Tesco, UK) cells were cultured in sterile YPD broth solution (50 g/L) and incubated for 16 h at a temperature of 37°C. After incubation, cells were washed using 280 mM D-mannitol and brought to a concentration of 2×10^7 cells/mL, then re-suspended in the CPMs. Human myelogeneous leukemic K562 cells (LGC Standards, Teddington, UK) were cultured in RPMI 1640 media at 37°C, supplemented with 10% heat-inactivated FBS (Biosera, UK), 1% L-glutamine and 1% penicillin–streptomycin. Cells were washed twice in 10 mL low conductivity KCl DEP buffer medium with 8.5% sucrose and 0.3% dextrose. HeLa cells were cultured in modified Eagle medium solution (Biosera, UK) supplemented with 10% heat-inactivated FBS (PAA, Pasching, Austria), 1% L-glutamine and 1% penicillin–streptomycin (Sigma Aldrich, UK) were required. When these adherent cells reached 70% confluence they were then trypsinised in the incubator for 3 min using 2 mL of trypsin/EDTA (Sigma Aldrich, UK), the trypsin effect was neutralised by adding 2 mL of fresh medium, a cell count was done and then the cell suspension was centrifuged at 1200 rpm for 7 min. Just prior to mixing with CPM, cells were washed twice in 10 mL low conductivity KCl DEP buffer medium with 8.5% sucrose and 0.3% dextrose. Cell counts were performed using a hemocytometer and were diluted to make a final concentration of $\sim 1 \times 10^6$ cell/mL for both HeLa and K562 populations. Viability tests were carried out before and after each experiment using trypan blue exclusion analysis.

2.5 Water content of CPM hydrogels

Microscope slides were washed with 70% ethanol followed by DI water; once dried the slides were weighed on precision scales (Ohaus Scout). An AZ210 UV light box (Mega Electronics, UK) was used to cross-link the CPMs of pre-polymer solutions. Fifty microlitres of each pre-polymer solution was dispensed on a separate slide, placed in the light box and irradiated for 50 s. Once the exposure was complete, DI water (100 μL) was dispensed over each slide while observing whether the pre-polymer had cross-linked or not by visual inspection of changes from liquid to gel phase. The slides were weighed again after cross-linking in order to find the weight of hydrogels in their hydrated phase. All the slides were placed in a dessicator and left for 17 h at 21°C to dehydrate, after which the weight of the slides were taken for a third time. The water percentage was calculated using the following formula:

$$water\ (\%) = \frac{w_{\text{hydrated}} - w_{\text{dehydrated}}}{w_{\text{hydrated}}} \times 100 \quad (3)$$

where w_{hydrated} is the initial weight of the hydrated gel after initial cross-linking and $w_{\text{dehydrated}}$ is the weight of dehydrated cross-linked hydrogel in units of grams. Water content experiments for each CPM was repeated four times and averaged to obtain the water content percentage.

2.6 Influence of PEG-DA viscosity on nDEP displacement

Using a rapid DEP characterisation protocol described elsewhere [31], the dielectrophoretic spectra of yeast suspended in PEG-DA at a medium conductivity of 7 mS/m, was performed to determine the frequency response for strong nDEP. Each CPM was mixed with 0.1% v/v of yeast stock solution ($\sim 1 \times 10^6$ cells/mL) and 50 μL of the prepared solution was deposited within the DEP microelectrode system. Images were captured under a light microscope (Eclipse E400 fluorescence, Nikon, Tokyo), connected to a CCD camera (Photonic Science, Cambridge). The imaging acquisition and analysis software (Photolite) captured DEP experiments every 5 s for 5 min for each sample of pre-polymer solution. A control sample of DI water buffered with KCl to 7 mS/m

and yeast cells was also analysed. Images were subsequently processed offline.

Kinematic viscosity (ν) measurements of PEG-DA% v/v between 0 and 50% were performed using PSL BS/U glass capillary viscometers (Rheotek). All following measurements were performed at room temperature (20°C) measured with a mercury thermometer. PEG-DA mixtures (50 mL) were made up and diluted appropriately with DI water. Each mixture (~25 mL) was poured into the viscometer via the larger channel and using a bulb on the opposite end, the mixture is lifted to its starting position through the glass capillary on the narrower channel side. The time taken for the fluid to flow downwards, between two marked points is recorded with a stopwatch. Readings were taken three times, averaged and multiplied by a nominal constant, either 0.095 or 0.011 mm^2/s for D- and B-type viscometers, respectively. To calculate the dynamic viscosity (μ) of each mixture according to (4), the fluid densities (ρ) were measured:

$$\nu = \frac{\mu}{\rho} \tag{4}$$

A glass container with a mass of 40.68 g was carefully filled with 21 mL of PEG-DA/water mixtures, measured using a graduated cylinder, ensuring all fluid was decanted. Between each reading the container was oven dried, with three readings taken per fluid sample. The average fluid density obtained for each mixture concentration was used to calculate the dynamic viscosity of our CPMs.

2.7 Viability of encapsulated cells in PEG hydrogels

The optimal PEG-DA concentration was mixed with 0.01% v/v of DMPA from the stock solution and with 0.1% v/v of yeast cells solutions. Cell aggregation and encapsulation was carried out over 4 min (3.5 min patterning and 30 s UV exposure using the UV irradiating DEP box described in Section 2.1), with the signal still applied to the electrode system, ensuring cells aggregate at the centre of each dot aperture. The resultant hydrogel was removed carefully and placed on a microscope slide to assess viable cells through the addition of 5 μL of a trypan blue (Sigma Aldrich, UK). The hydrogels were cultured and incubated to monitor cell viability every 24 h for 1 week. These experiments ($n = 4$) were carried out on yeast, K562 and HeLa PEG-DA encapsulated aggregates.

3 Results and discussion

3.1 Mechanical effects of varying hydrogel water content

The water percentage was calculated by finding the difference in weight for each PEG-DA concentration in its hydrated and dehydrated phase, with the assumption that the difference in weight was due to loss of water [32]. Analysing the water content of various PEG-DA concentrations up to 50% CPM showed that as the concentration of PEG-DA increased in the CPM, the water content in the polymerised solution decreased in an approximately linear fashion, as shown in Fig. 2. This correlated well with the assumption that for a given PEG-DA concentration, the remaining volume taken up in the CPM must be water. Previous studies investigating the swelling of PEG-DA solutions in the range of 1–10% concluded that an increase in the macromer concentration led to a decrease in water content [33]. From the graph, it can be seen that PEG-DA concentrations between 5 and 30% have a water content in line with that of tissue and the ECM (>70%), which would favour the microenvironment of embedded cells for growth, proliferation and possible migration [34]. However, the 5–10% PEG-DA could not be used due to their brittleness upon handling and removal from microsystem. Above 10% PEG-DA concentration, the water content of the hydrogels was lower and easier to peel off the microelectrode chip. Gel concentrations >25% were found to be significantly more sturdy (i.e. not easily cracked upon handling or more solid) than those with concentrations <25%, most likely due to the more porous hydrogel's (<25%) ability to mimic the structure and water content of the native ECM found in living tissues [35]. In general, as the pre-polymer concentration and viscosity of the continuous phase solution increased, the hydrogel's mechanical stability and handling capabilities improved.

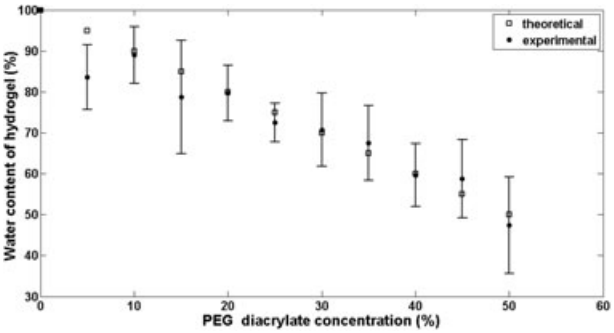

Figure 2. Theoretical and experimental values of hydrogel water content versus PEG-DA pre-polymer concentrations.

3.2 Effect of viscosity on nDEP patterning

Evaluation and optimisation of DEP patterning required that the DEP force on a cell is able to overcome the viscous effects of the CPM. Figure 3 shows the experimental and best-fit dielectrophoretic spectra of a homogeneous population of yeast cells suspended in 15% PEG-DA with 280 mM D-mannitol at 7 mS/m. The spectrum was obtained using a multichannel signal generator on DEP-dot electrodes designed for parallel characterisation experiments [31]. The multi-shelled model describing yeasts' concentric compartments was used to fit the experimental data to the theoretical model [30]. From the spectrum, it can be seen that the frequency at which there is a

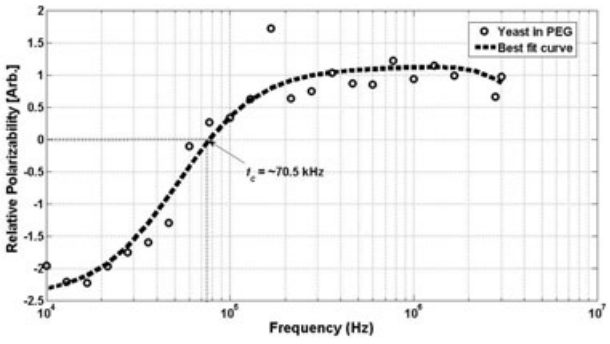

Figure 3. Acutal DEP spectrum of yeast cells (o) suspended in 15% PEG-DA ($\sigma_m = 7$ mSm) and the best-fit curve (—) based on a fitting algorithm [30] showing a crossover frequency at 70.5 kHz.

transition from nDEP to pDEP (i.e. the crossover frequency) is situated at (f_c) = ~70.5 kHz. As we require a strong nDEP force with the current experimental parameters, a signal at the lower end of the frequency spectrum ($20V_{p\text{-}p}$, 10 kHz) was applied to investigate the efficiency of nDEP aggregation for yeast cells suspended in different ratios of CPMs. From Castenallos et al., the low ionic conductivity solution used here, $\sigma_m = 7$ mS/m, gives an incremental temperature rise calculated to be 0.7°C [36]. Hence, a temperature rise of less than 2°C in our system means electrothermal forces can be neglected.

Figure 4A shows viscosity measurements of CPMs versus kinematic and dynamic viscosities, measured at 20°C. It can be seen that the measured viscosity of water (0.008 Pa s) is approximately ~4.5′ lower than that of 30% PEG-DA and increases to ~12′ at 50% PEG-DA. Empirical results show nDEP patterning was significantly more effective at PEG-DA concentrations below 30%, with the nDEP forces unable to effectively transport cells in PEG-DA concentrations greater than 30% within a 5 min time period. Yeast cells randomly dispersed within the 150 μm DEP-dot system were concentrated radially towards the centre of the dot aperture, where field energies are at a minimum, under the influence of an axisymmetrical nDEP force field.

To evaluate the efficiencies of the DEP patterning process we used an average displacement ratio defined in Eq. (5). The average displacement ratio (s_r) is the quantity describing the radial packaging efficiency of cell aggregates ($R_{AGGREGATE}$) within each dot region as a ratio to the dots radius (R_{DOT}), formed due to nDEP. This ratio was calculated at 30 s intervals over 3 min (Fig. 4B), and averaged over four cardinal points.

$$s_r = \frac{R_{DOT} - R_{AGGREGATE}}{R_{DOT}} \quad (5)$$

In general, s_r values were found to increase over time for PEG-DA concentrations less than 30%. At 5% PEG-DA concentration, s_r over 30 s was 0.38 reaching a final s_r of 0.68 indicating a aggregate formation rate of 0.002 s^{-1}. The rate of aggregate formation in 25% PEG-DA concentration between 30 s ($s_r = 0.2$) and 180 s ($s_r = 0.3$) was 0.00067 s^{-1}, a threefold

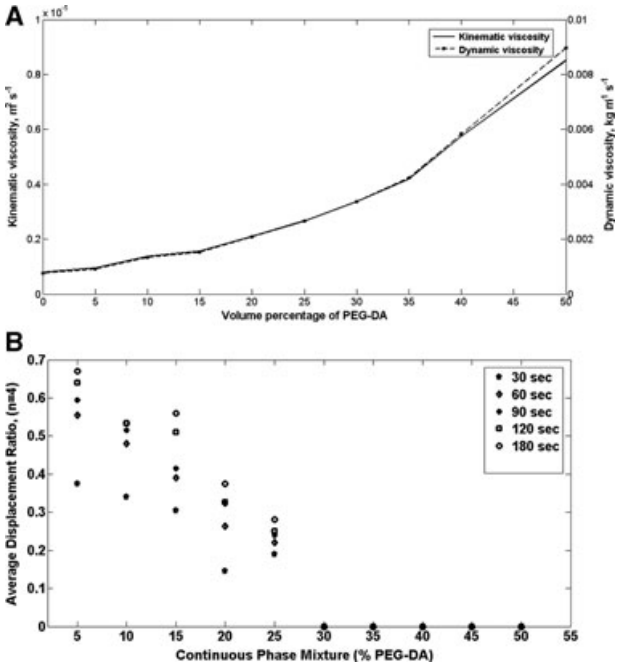

Figure 4. (A) Measured viscosity data (kinematic and dynamic) of various PEG-DA mixtures with water, up to 50% v/v concentrations at 20°C. Assuming water has a known dynamic viscosity of ~0.001 kg m^{-1} s^{-1}, 4% error in this measurement was seen, which can be assumed to be constant. (B) Average displacement ratio (s_r) of yeast cells subjected to an nDEP force ($20V_{p\text{-}p}$, 10 kHz) at CPM of 5–50% PEG-DA concentrations over 180 s observation.

decrease in the rate of aggregate formation in comparison to 5% PEG-DA. Pre-polymer PEG-DA concentrations between 10 and 15% showed relatively comparable s_r values over time ($s_r = 0.57 \pm 0.05$ at 180 s) before exhibiting a significant drop in efficiency in 20% PEG-DA to an s_r value of 0.38. The rate of aggregate formation between 30 and 180 s for 10 and 15% PEG-DA were 0.00133 and 0.00167 s^{-1}, respectively. Although particle translation due to DEP was not observed for CPM ≥ 30% over a 5 min time period, an extended period of time might reveal particle motion. The fourfold increase in CPM viscosity logically suggests that an nDEP force the cell experiences is counteracted by the increased viscous force, slowing its movement down as it transverses the CPM. By considering Stokes law, the DEP velocity (u_{DEP}) of a spherical cell of diameter (d_p) due to a dielectrophoretic force can be seen to be influenced by the continuous phase viscosity, μ_{CPM} from Eq. (6):

$$\frac{F_{DEP}}{3\pi d_p \mu_{CPM}} \quad (6)$$

Based on the viscosity measurements obtained in Fig. 5A, an order of magnitude displacement based on the instantaneous particle velocity for a yeast cell ($d_p = 8$ μm) can be estimated. With an electric field strength determined a distance away from the electrode edge, and assuming the relative permittivity of the medium is the same as water ($\varepsilon_r = 78$), at the dot centre, that is 75 μm away from the electrode edge, the

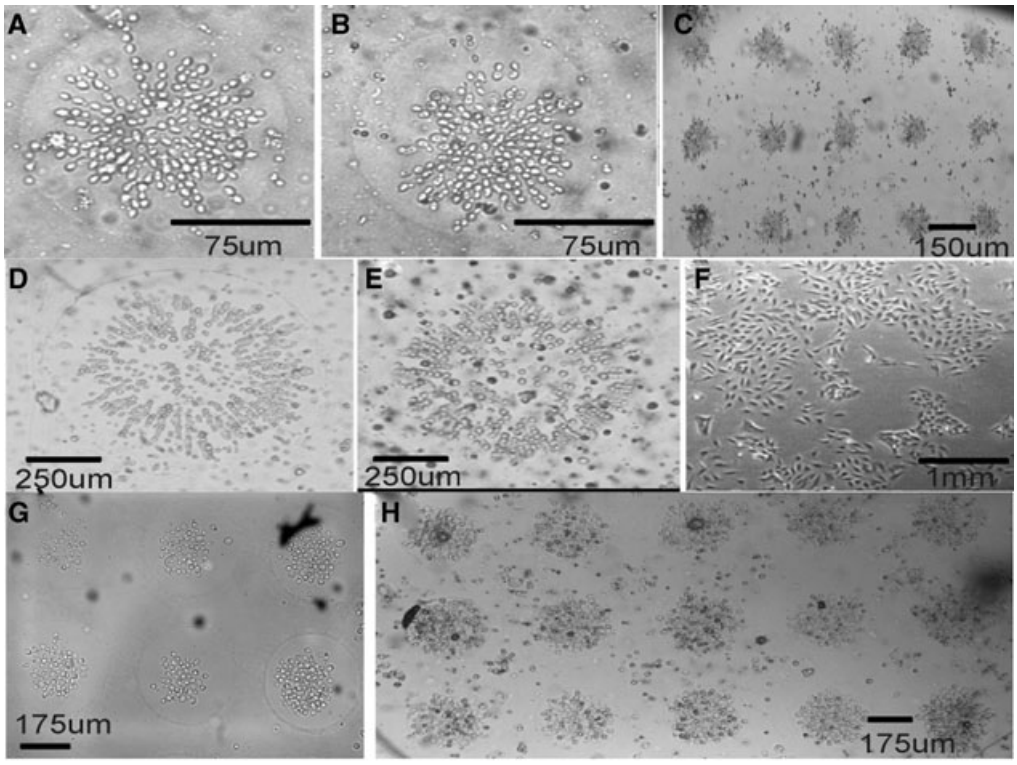

Figure 5. Different patterned cell aggregate arrays encapsulated in photo-polymerised PEG-DA for yeast cells (A–C); human myelogenous leukemic cells (D, E); and HeLa cells (F–H). (A) A 20′ magnification of a single cluster of yeast cells upon initial cross-linking of 15% PEG-DA, while in (B) a cluster stained with trypan blue a day after cross-linking (darker cells indicate non-viable and lighter cells viable); (D) K562 cells initially cross-linked in 15% PEG-DA and (E) 4 days after cross-linking with lighter cells viable and darker cells non-viable; (F) HeLa cells attached to the culture flask and when initially cross-linked in the hydrogel (G) they are more spherical; (H) a larger array of HeLa clusters evenly spaced within the hydrogel scale bars included for each image.

particle velocity for different CPMs were calculated as 0.082, 0.043, 0.019 and 0.0073 μm/s for 0, 15, 30 and 50% PEG-DA, respectively. Closer to the electrode edge (10 μm away) particle velocities were found to be of the order of 4.5, 2.4, 1.1 and 0.41 μm/s for 0, 15, 30 and 50% PEG-DA, respectively. The exponential decay of the electric field gradient away from the electrode edge in this quasi-3D system is complex and would need to be solved for different particle trajectories at various positions. Another contributing factor to the decrease in aggregate formation rate could be due to changes in medium permittivity. PEG-DA has a lower permittivity than water and changes in CPM composition would have an effect on this, thus affecting the Clausius–Mossotti factor. From our results it was observed that patterning was possible at CPMs of 5–25%. Efficient patterning was achieved with solutions in the range of 5–15%, where the aggregate formation was broadly similar to cells patterned in the water control sample. nDEP on K562 and HeLa cells, in the same medium conductivity, was carried out at 10 and 5 kHz, respectively.

3.3 Aggregate viability within hydrogels

Using the 15% CPM, cell aggregates were formed on the dot microelectrode array with nDEP and photo-polymerised within the purpose-built UV DEP light box with a 30 s uniform exposure. For the suspension cells, Fig. 5A–C shows yeast cells embedded in cross-linked PEG-DA while Fig. 5D and E shows K562 cells. The non-spherical adherent HeLa cells, prior to trypsinisation from the culture flask, can be seen in Fig. 5F, and examples of patterned arrays of HeLa cells can be seen in Fig. 5G and H. Cell viability was assessed after hydrogel formation to determine the effects of UV irradiation and free radical formation. The hydrogels were maintained in sucrose dextrose solution, which was refreshed every 24 h and incubated at 37°C. Viability was determined every 24 h for a week using trypan blue exclusion to identify viable and non-viable cells. Each cluster of cells had an average cell number of 110 ± 7 and counts performed an average of three times for live and dead cells. Figure 6A shows the average viability of yeast and K562 cells after patterning and encapsulation in 15% PEG-DA. With an initial viability of 92% upon hydrogel formation, yeast aggregates showed a mean viability of 87% by the end of the week. In comparison, K562 cells were more robust showing a mean viability of 97% on the first day dropping to 93% by the end of the week. Figure 6B shows the viability results of encapsulated HeLa cells, revealing a starting viability of $99 \pm 1\%$ that falls to $88 \pm 2.65\%$ by the seventh day of observation. These results indicate that possible long-term cell viability of cells could be attained with our process.

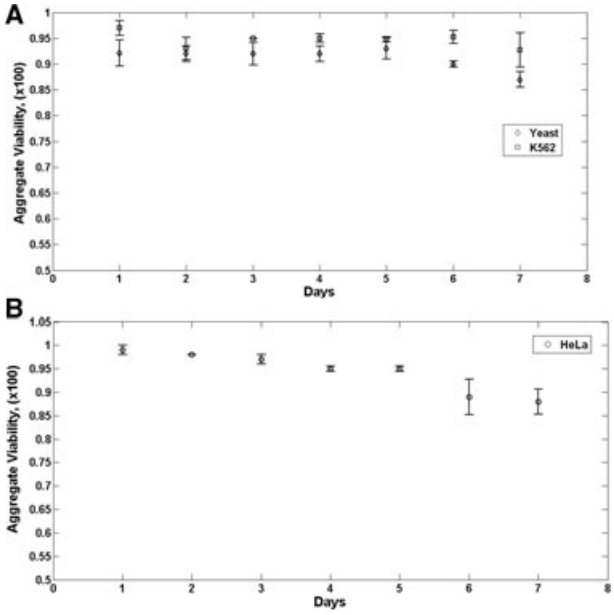

Figure 6. (A) Average viability for patterned and encapsulated yeast and K562 cells in the optimised PEG-DA hydrogel, maintained over a period of 7 days, showing a relative viability decrease of ∼5%. (B) Viability of HeLa cells over a 7 day period with a starting value of 99 ± 1%, which falls to 88 ± 2.65% at the end of the observation period.

The protocol used to pattern and encapsulate cells did not pose significant harm or affect the viability of the cells. This could possibly be due to the low-energy trapping regions cells were directed towards, the low UV exposure period employed in comparison to other studies and the use of a significantly lower dose of photo-initiator to catalyse hydrogel formation [10, 18]. Bryant et al. showed that the choice of photo-initiator for cell encapsulation systems has varying effects on cytocompatibility [37]. They compared the cytotoxic effects of several photo-initiators (UV and visible) on a fibroblast cell line (NIH/3T3) and found that at low photo-initiator concentrations (≤0.01% w/w), DMPA had a relative survival of ∼50%, whereas Liu and Bhatia used a threefold increase in photo-initiator concentration compared to our study, in the PEG-DA encapsulation of a human hepatoma cell line (HEPG2) [10]. As an overestimation, due to the absence of PEG-DA as a free radical sink (experiments were performed in culture media), they found that photo-initiator concentrations >0.9 mg/mL (i.e. 0.09% v/v) in combination with UV exposure times had toxic effects on the cell. When cell viability was assessed in the 3D hydrogel, relative spatial distribution of viable cells was seen to be uniform. Though highly dependent on cell type, to reduce cytotoxic effects in our experiments a ninefold reduction in photo-initiator concentration was used in the CPM. Upon initial cross-linking of the pre-polymer, relative cell viability over the period of observation for our test cells were high at > 85%, compared with an 80 ± 7% over 14 days for chrondrocytes experiencing pDEP as described by Albrecht et al. [18].

3.4 Optimisation outputs

The optimisation study began by finding the mechanical effects of varying PEG-DA concentrations in CPMs; this was done in order to pick concentrations that would form a hydrogel for easy peeling as well as maintaining a high water content that is suitable for maintaining cell viability. The range that favoured these two conditions was found between 15 and 25%. The next step was to find the range of CPM that would allow fast and effective nDEP patterning of cell aggregates. Our results showed that the range for that was between 5 and 25%, however according to the displacement ratio values there was a huge drop in the displacement ratio at concentrations ≥ 20% PEG, which brought down the usable range to 5–15% PEG. Combining the results between the two studies indicated that a pre-polymer solution of 15% appeared to be the optimal concentration for encapsulating cell aggregates by nDEP. Our preliminary evaluation of this process assessed the cell viability of yeast, K562 and HeLa cells, which show small drops in viabilities across the different cell types over a week period. This is a significant improvement in viability rates over those described in the literature, which may be attributable to the low dose of photo-initiator (by a factor of 3) used in comparison to other studies [10, 18].

4 Concluding remarks

In summary, we have presented a new approach for using repulsive dielectrophoretic forces combined with PEG-DA pre-polymer solution for cell patterning and encapsulation within our wide-area UV-irradiated DEP light box. The study was performed in order to assess the most compatible physical, chemical and electrical conditions for biological cell manipulation within our developed system. Fifteen percent PEG-DA pre-polymer solution was used to suspend three different cell types, and using nDEP forces, cells were patterned in the DEP-dot electrodes where cells formed circular aggregates at each dot centre in an array format. Viability assessment showed that the presented protocol was able to maintain a high viability over a period of seven days. Significantly, using this approach in which evenly spaced aggregates such as those presented in Fig. 5C and H, without the use of an additional separate photo-mask, forms distinct clusters that can be utilised as a platform for whole-cell biosensors or high-throughput drug screening using, for example, robotic spotting devices on a wide-area array. This system will be further characterised and assessed using multiple cell types and primary mammalian cells, where analysis and study of global cell behaviour between neighbouring cells over time and in response to drug doses could lead to a more cost effective and accurate 3D model for therapeutic and drug discovery studies.

The authors have declared no conflict of interest.

5 References

[1] Nederman, T., *Cancer Res.* 1984, *44*, 254–258.

[2] Bryant, S. J., Anseth, K. S., *J. Biomed. Mater. Res.* 2002, *59*, 63–72.

[3] Aubin, H., Nichol, J. W., Hutson, C. B., Bae, H., Sieminski, A. L., Cropek, D. M., Akhyari, P., Khademhosseini, A., *Biomaterials* 2010, *31*, 6941–6951.

[4] Wichterle, O., Lim, D., *Nature* 1960, *185*, 117–118.

[5] VandeVord, P. J., Matthew, H. W. T., DeSilva, S. P., Mayton, L., Wu, B., Wooley, P. H., *J. Biomed. Mater. Res.* 2002, *59*, 585–590.

[6] Scott, R. A., Peppas, N. A., *Biomaterials* 1999, *20*, 1371–1380.

[7] Koh, W. G., Pishko, M., *Mater. Res. Soc. Symp. Proc.* 2002, *723*, 141–146.

[8] Yang, S. F., Leong, K. F., Du, Z. H., Chua, C. K., *Tissue Eng.* 2001, *7*, 679–689.

[9] Drury, J. L., Mooney, D. J., *Biomaterials* 2003, *24*, 4337–4351.

[10] Liu, V. A., Bhatia, S. N., *Biomed. Microdevices* 2002, *4*, 257–266.

[11] Namba, R. M., Cole, A. A., Bjugstad, K. B., Mahoney, M. J., *Acta Biomater.* 2009, *5*, 1884–1897.

[12] Cruise, G. M., Hegre, O. D., Lamberti, F. V., Hager, S. R., Hill, R., Scharp, D. S., Hubbell, J, A., *Cell Transplant.* 1999, *8*, 293–306.

[13] Sawhney, A. S., Pathak, C. P., Hubbell, J. A., *Biomaterials* 1993, *14*, 1008–1016.

[14] Pethig, R., Menachery, A., Heart, E., Sanger, R. H., Smith, P. J. S., *IET Nanobiotech.* 2007, *2*, 31–38.

[15] Pohl, H. A., *J. Appl. Phys.* 1951, *22*, 869–871.

[16] Voldman, J., *Annu. Rev. Biomed. Eng.* 2006, *8*, 425–454.

[17] Kang, Y., Li, D., *Microfluid. Nanofluid.* 2009, *6*, 431–460.

[18] Albrecht, D. R., Underhill, G. H., Wassermann, T. B., Sah, R. L., Bhatia, S. N., *Nat. Methods* 2006, *3*, 369–375.

[19] Lin, R. Z., Ho, C. T., Liu, C. H., Chang, H. Y., *Biotech. J.* 2006, *1*, 949–957.

[20] Broche, L. M., Bhadal, N., Lewis, M. P., Porter, S., Hughes, M. P., Labeed, F. H., *Oral Oncol.* 2007, *43*, 199–203.

[21] Hughes, M. P., Morgan, H., Rixon, F. J., Burt, J. P. H., Pethig, R., *Biochim. Biophys. Acta* 1998, *1425*, 119–126.

[22] Sanchis, A., Brown, A. P., Sancho, M., Martinez, G., Sebastian, J. L., Munoz, S., Miranda, J. M., *Bioelectromagnetics* 2007, *28*, 393–401.

[23] An, J., Lee, J., Lee, S. H., Park, J., Kim, B., *Anal. Bioanal. Chem.* 2009, *394*, 801–809.

[24] Fatoyinbo, H. O., Hughes, M. P., Martin, S. P., Pashby, P., Labeed, F. H., *J. Environ. Monit.* 2007, *9*, 87–90.

[25] Suzuki, M., Yasukawa, T., Mase, Y., Oyamatsu, D., Shiku, H., Matsue, T., *Langmuir* 2004, *20*, 11005–11011.

[26] Kaji, H., Hashimoto, M., Nishizawa, M., *12th International Conference on Miniaturized Systems for Chemistry and Life Sciences*, San Diego, California, USA 2008.

[27] Tsutsui, H., Yu, E., Marquina, S., Valamehr, B., Wong, I., Wu, H., Ho, C. M., *Ann. Biomed. Eng.* 2010, *38*, 3777–3788.

[28] Albrecht, D. R., Sah, R. L., Bhatia, S. N., *Biophys. J.* 2004, *87*, 2131–2147.

[29] Mellott, M. B., Searcy, K., Pishko, M. V., *Biomaterials* 2001, *22*, 929–941.

[30] Fatoyinbo, H. O., Hoettges, K. F., Hughes, M. P., *Electrophoresis* 2008, *29*, 3–10.

[31] Fatoyinbo, H. O., Kadri, N. A., Gould, D. H., Hoettges, K. F., Labeed, F. H., *Electrophoresis* 2011, *32*, 2541–2549.

[32] Benamer, S., Mahlous, M., Boukrif, A., Mansouri, B., Youcef, S. L., *Nucl. Instrum. Methods Phys. Res. B* 2006, *248*, 284–290.

[33] Sipics, J., Libera, M., *Bioengineering Conference, 2005. Proceedings of the IEEE 31st Annual Northeast*, Stevens Inst Technol, Hoboken, NJ 2005, 204–205.

[34] Alberts, B., Johnson, A., Lewis, J., Raff, M., Roberts, K., Walter, P., *Molecular Biology of the Cell*, Garland Science, Taylor & Francis Group, New York 2002.

[35] Russell, R. J., Axel, A. C., Shields, K. L., Pishko, M. V., *Polymer* 2001, *42*, 4893–4901.

[36] Castellanos, A., Ramos, A., Gonzalez, A., Green, N. G., Morgan, H., *J. Phys. D: Appl. Phys.* 2003, *36*, 2584–2597.

[37] Bryant, S. J., Nuttelman, C. R., Anseth, K. S., *J. Biomat. Sci.-Polym. E* 2000, *11*, 439–457.

